Band offsets at the interfaces between β-Ga_2O_3 and Al_2O_3

Sai Lyu *
School of Physics and Electronics, Shandong Normal University, Jinan 250358, China
and Shandong Provincial Engineering and Technical Center of Light Manipulations,
Shandong Normal University, Jinan 250358, China

(Received 17 August 2022; accepted 19 January 2023; published 30 January 2023)

The band offsets at the interfaces between $(\bar{2}01)$ β-Ga_2O_3 and Al_2O_3 polymorphs are calculated through hybrid functional calculations. For alumina, we consider four representative phases, i.e., α, κ, θ, and γ-Al_2O_3. We generate realistic slab models for the interfaces, which satisfy electron counting rules. The O atoms bridge the β-Ga_2O_3 and the Al_2O_3 slabs and the dangling bonds at the interfaces are saturated. The band offsets are obtained through an alignment scheme, which requires separate bulk and interface calculations. The calculated band offsets are useful for the design of devices based on the β-Ga_2O_3/Al_2O_3 heterojunctions, particularly β-Ga_2O_3 metal-oxide semiconductor field effect transistors.

DOI: 10.1103/PhysRevMaterials.7.014603

I. INTRODUCTION

Gallium oxide (Ga_2O_3) is a promising semiconductor material to advance existing technologies in the field of high-power electronics and solar-blind ultraviolet (UV) photodetectors due to its large band gap [1]. Among the five identified polymorphs of Ga_2O_3, β-Ga_2O_3 is the most stable phase and thus has attracted a great deal of recent attention [1]. This material has a wide band gap of 4.5–4.9 eV and its high breakdown electric field significantly exceeds that of the commonly used SiC and GaN [2,3]. Most importantly, bulk crystals of β-Ga_2O_3 can be produced by using melt growth techniques at a potentially lower cost than the fabrications of SiC and GaN [1,4].

Aluminum oxide (Al_2O_3) or alumina is widely used in many important technological applications such as high-κ dielectric material, substrate, and catalyst [5,6], Among all the polymorphs of Al_2O_3, the α phase, sapphire, is the most stable one in spite of pressure or temperature conditions [7]. Besides, some metastable phases, such as κ, θ, and γ, also exist [7]. These four representative phases of alumina are differing in atomic structures and physical properties [8]. The alloys between Ga_2O_3 and Al_2O_3 polymorphs have attracted a lot of recent attention [9–11]. Their interfaces are thus intriguing to study.

In the development of electronic devices based on β-Ga_2O_3, the fabrication of metal-oxide semiconductor field effect transistors (MOSFETs) has been recently demonstrated [12–15]. For β-Ga_2O_3 MOSFETs, a semiconductor with a high dielectric constant (high κ) is suitable to serve as a gate dielectric so as to reduce the device operating voltage [16,17]. Moreover, a gate dielectric must provide sufficient barriers to limit both electrons and holes, which requires a sufficiently large band gap to obtain the desired band offsets ($\gtrsim$1 eV) [17]. Al_2O_3 has been identified as a good candidate in terms of its large band gap and high dielectric constant [1,5,6]. Recently, Kamimura *et al.* obtained a conduction band offset (CBO) of 1.5 eV and a corresponding valence band offset (VBO) of 0.7 eV at the α-Al_2O_3/β-Ga_2O_3 (010) interface [16]. In Ref. [17], the VBO was measured to be 0.07 eV for atomic layer deposited (ALD) α-Al_2O_3 on $(\bar{2}01)$ β-Ga_2O_3 and -0.86 eV for sputtered α-Al_2O_3 on Ga_2O_3. And the corresponding CBO was measured to be 2.23 eV and 3.16 eV, respectively. Hung *et al.* found a CBO of 1.7 eV on atomic layer deposited Al_2O_3/Ga_2O_3 $(\bar{2}01)$ interface through capacitance-voltage measurements [18]. Hattori *et al.* measured VBO of 0.5 eV and the CBO of 1.9 eV, respectively, at the γ-Al_2O_3/β-Ga_2O_3 (010) interface [19].

Band offsets are critical parameters for designs of heterostructures. However, the reported values for both VBO and CBO at the Al_2O_3/β-Ga_2O_3 interfaces clearly exhibit a large variability. Take the VBO at the Al_2O_3/β-Ga_2O_3 interface as an example, the reported value vary as much as 1.5 eV. Such an ambiguity is also found for some other dielectrics deposited on β-Ga_2O_3 [1]. Some possible reasons include interface disorder, surface termination, and so on [1]. Besides, the band offsets between Ga_2O_3 and some Al_2O_3 polymorphs were theoretically estimated based on the electron affinity rule [9–11]. However, it is well known that the band offsets at the interfaces between two compounds are affected by many other factors, e.g., strain, chemical bonding, etc., which can significantly deviate the offsets values from those calculated from the electron affinity rule. This makes that the simulations of interfaces are necessary to accurately determine the corresponding band offsets [20,21]. Given the above, there is a clearly a need to elucidate the atomic structures and the chemical bondings at these interfaces. Besides, most of the recent studies are limited to the α phase, without considering other phases, which also have large band gaps and high dielectric constants [5,6]. Therefore, computational investigations are required to compliment experiment and accurately determine the band offsets at the defect-free interfaces between β-Ga_2O_3 and Al_2O_3 polymorphs.

*sailyu@sdnu.edu.cn

 ©2023 American Physical Society

In this study, we computationally investigate the interfaces between β-Ga_2O_3 and Al_2O_3 using density functional theory (DFT). We investigate four representative phases of Al_2O_3, i.e., α, θ, κ, and γ. To avoid the band-gap problem for DFT, we employ hybrid density functional to determine the electronic band structure. The band offsets are obtained through an alignment scheme in which bulk calculations and interface calculations are combined [21]. Our study can provide guide for future synthesis and device design, especially for the design of β-Ga_2O_3 MOSFETs.

II. METHODS

Our DFT calculations are performed by using the CP2K code [22]. The implemented Gaussian plane waves (GPW) method can efficiently solve the Kohn-Sham equation [23] by using Gaussians as basis set and plane waves (PW) as auxiliary basis. We use double-ζ basis sets [24] and Goedecker–Teter–Hutter (GTH) [25] pseudopotentials for all the atoms. Treating the Ga 3*d* electrons as valence is important to appropriately describe its electronic band structure [9]. The energy cutoff of PW expansion is 600 Ry and the Brillouin zone is sampled by the Γ point when a sufficiently large supercell ($\gtrsim$100 atoms) is used in the calculations. Besides, in the bulk calculations of the indirect-gap semiconductors, i.e., β-Ga_2O_3 and θ-Al_2O_3, the band gaps are determined using finite Monkhorst-Pack k-point meshes [26], i.e., $4\times12\times8$. More computational details can be found in the Supplemental Material [27]. The geometry optimizations use the generalized gradient approximation developed by Perdew, Burke, and Ernzerhof (PBE) [28]. The established experimental band gaps of β-Ga_2O_3 and Al_2O_3 are reproduced through a common approach of adjusting the fractions α of Fock exchange in the PBE0(α) hybrid functionals [29,30]. In the PBE0(α) calculations, auxiliary density matrix method adopted to accelerate the time-consuming Fock exchange calculations [31].

The band offsets at the interfaces are determined through the alignment procedure described in Refs. [21,32,33]. For a heterojunction A/B, this procedure requires an interface calculation and another two bulk calculations for two interface components. To be more specific, the VBO of a heterojunction A/B is calculated from the following equation:

$$\mathrm{VBO}(A/B) = \left(E^B_{\mathrm{VBM}} - \bar{V}^B\right) - \left(E^A_{\mathrm{VBM}} - \bar{V}^A\right) + (\bar{V}^B - \bar{V}^A), \tag{1}$$

where $E_{\mathrm{VBM}} - \bar{V}$ is the valence band maximum (VBM) versus the bulk reference level obtained from bulk calculations, and $\bar{V}^B - \bar{V}^A$ denotes the interface lineup of bulk reference levels determined in the interface calculation [34]. We follow the common practice of choosing the averaged electrostatic potential as the bulk reference level. The corresponding CBO can then be calculated from the following equation:

$$\mathrm{CBO}(A/B) = \left(E^B_{\mathrm{g}} - E^A_{\mathrm{g}}\right) + \mathrm{VBO}(A/B), \tag{2}$$

where E_{g} denotes the band gap of each interface component. The lineup at the interface is calculated at the GGA level, which can yield almost the same interface lineup as hybrid functionals but be less computationally expensive [20,21,35,36]. To determine the interface lineup, we first average the electrostatic potential in the *xy* plane (the interface plane) and then apply a double convolution along the *z* direction vertical to the *xy* plane [33,37]. In the interface models, the asymmetric slabs give rise to finite electric fields across the interfaces under the periodic boundary conditions [38]. To get the interface lineup not affected by the built-in electric fields, we follow the extrapolation scheme developed by Foster *et al.* [39]. In this scheme, the macroscopically averaged electrostatic potential for each interface component is extrapolated from its bulk-like region to the nominal interface position. Herein we take the midway between the surface Ga layer and Al layer as the nominal interface position. The interface lineup is obtained by calculating the difference between two extrapolations at the nominal interface position. This extrapolation scheme has been successfully applied to the interfaces between wurtzite III-N (III=Al, Ga) and β-Ga_2O_3 [34].

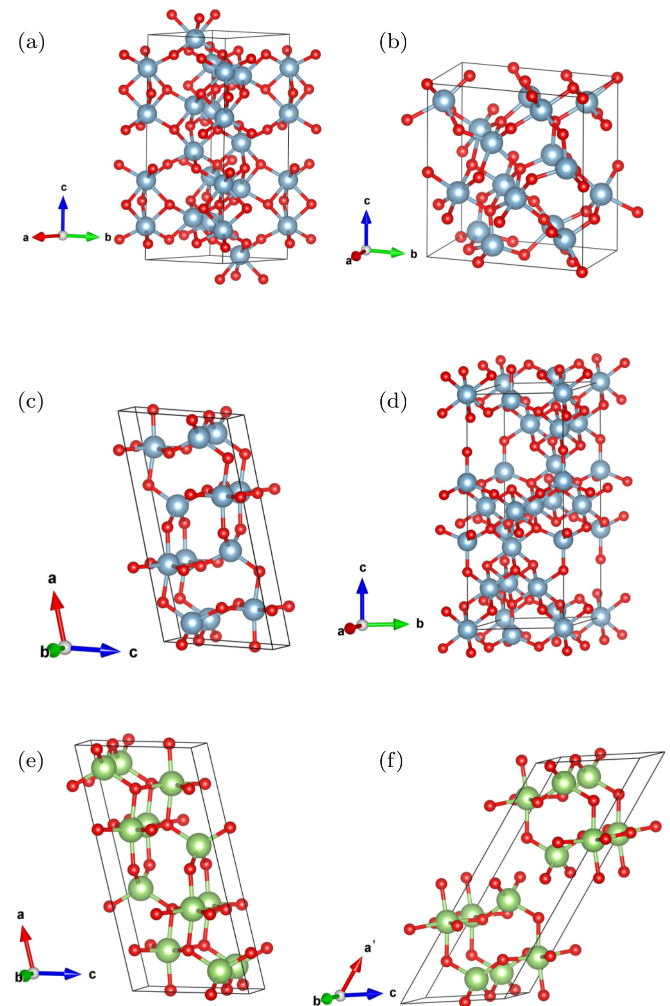

FIG. 1. Unit cells of β-Ga_2O_3 and Al_2O_3. (a) α-Al_2O_3 (hexagonal), (b) κ-Al_2O_3 (orthorhombic), (c) θ-Al_2O_3 (monoclinic), (d) γ-Al_2O_3 (hexagonal), and (e) β-Ga_2O_3 (conventional monoclinic unit cell), (f) β-Ga_2O_3 (transformed monoclinic unit cell, $\mathbf{a}' = \mathbf{a} + 2\mathbf{c}$). The red, green, and grey spheres indicate O, Ga, and Al atoms, respectively.

TABLE I. Lattice constants, band gaps (in eV), and VBM levels (in eV) of α, κ, θ, γ-Al_2O_3, and β-Ga_2O_3. The band gaps and the VBM positions are calculated at the PBE0(α) level in which the mixing parameter α for each material is also given.

	α-Al_2O_3		κ-Al_2O_3		θ-Al_2O_3		γ-Al_2O_3		β-Ga_2O_3	
	Calc.	Exp.	Calc.	Exp.	Calc.	Exp.	Calc.	Exp.	Calc.	Exp.
a (Å)	4.80	4.76 [54]	4.88	4.84 [55]	11.88	11.85 [42]	5.67	5.61 [43]	12.22	12.21 [56]
b (Å)			8.43	8.31	2.95	2.90			3.06	3.03
c (Å)	13.10	12.99	9.02	8.94	5.69	5.62	13.94	13.75	5.82	5.79
β					104.14°	103.83°			103.84°	103.83°
PBE0(α)	0.30		0.29		0.29		0.39		0.27	
E_{gap}^{direct} (eV)	8.78	8.8 [57]	7.67		7.61		7.60	7.6 [58]	4.81	4.76 [59]
$E_{gap}^{indirect}$ (eV)					7.22				4.80	
VBM	4.08		3.86		3.04		3.20		2.94	

III. RESULTS AND DISCUSSION

In Fig. 1, we show the units cells of the four phases of Al_2O_3 (α, κ, θ, and γ) and β-Ga_2O_3 studied in this paper. For a structural model of α-Al_2O_3, the Al cations occupy the octahedral sites and the O anions are in the vertices of octahedrons. Its space group belongs to $R\bar{3}c$. When represented by a hexagonal lattice as shown in Fig. 1(a), α-Al_2O_3 contains alternative Al and O layers. In the case of κ-Al_2O_3, the Al cations occupy either octahedral sites or tetrahedra sites surrounded by the O anions. The crystal structure of κ-Al_2O_3 corresponds to the space group $Pna2_1$ in the orthorhombic class [40,41]. Monoclinic θ-Al_2O_3 has a space group of $C2/m$ with the Al cations on either octahedral and tetrahedra sites [42]. The model of θ-Al_2O_3 is based on the crystal structure determined in Ref. [42]. For γ-Al_2O_2, we use a 40-atom hexagonal cell comprising eight Al_2O_3 units. The O anions sublattice is fully occupied and two Al octahedral sites are unoccupied, which are farthest from each other. This model is derived from the cubic spinel structure with a lattice constant of 7.9 Å refined in Ref. [43], and for more details of the model construction, we refer to Refs. [44,45]. The experimental lattice constants a and c for this hexagonal model are derived to be 5.61 Å and 13.75 Å, respectively. β-Ga_2O_3 belongs to monoclinic crystal structure with the Ga cations belonging to either distorted tetrahedra or distorted octahedra [3,46]. It has the same space group with θ-Al_2O_3, i.e., $C2/m$, making it easily form alloys with θ-Al_2O_3 [9,47]. The lattice parameters of the bulk β-Ga_2O_3 and the four phases of Al_2O_3 are obtained through fully geometry optimizations with the GGA functional, which are summarized in Table I. The corresponding experimental lattice parameters and band gaps are also given. The band gaps and VBM positions with respect to the bulk reference levels are obtained through PBE0(α) calculations.

In experimental studies of the band offsets between β-Ga_2O_3 and gate dielectrics, β-Ga_2O_3 is commonly taken as the substrate. Here we focus on the technologically important ($\bar{2}01$) surface of β-Ga_2O_3 for which numerous studies have been conducted to find appropriate gate dielectrics [1]. Because of the lattice mismatches between Al_2O_3 and β-Ga_2O_3, the in-plane lattice constants of Al_2O_3 are controlled by the ($\bar{2}01$) β-Ga_2O_3 substrate. The biaxial strain due to the lattice mismatches causes the Al_2O_3 epilayer adopt new out-of-plane lattice parameters. Since the epitaxial relationships between Al_2O_3 and ($\bar{2}01$) β-Ga_2O_3 have not been experimentally reported, we theoretically investigate them by explicitly taking account into the chemical bondings at the interfaces, the electron counting rule [48–51], and the lattice mismatches. We use oxygen atoms to bridge Al_2O_3 and ($\bar{2}01$) β-Ga_2O_3 as interfacial O atoms can admit more flexible bondings than cations [34,50,52,53]. In β-Ga_2O_3, the Ga layer and the O layer is alternating along the direction perpendicular to the ($\bar{2}01$) surface of β-Ga_2O_3. Under the requirement of the electron counting rule, the Al layer and the O layer should also be alternating along the direction vertical to the orientation of Al_2O_3. In addition, the electron counting rule requires that the Al layer and the Ga layer should have the same number of cations. Under these conditions, we then determine the epitaxial relationships between Al_2O_3 and ($\bar{2}01$) β-Ga_2O_3 which leads to minimal lattice mismatches. A similar procedure was successfully applied to the interfaces between III-N (III = Al, Ga) and β-Ga_2O_3 [34]. To validate the above procedure in the present study, we apply it to determine the epitaxial relationships between α-Al_2O_3 and ($\bar{2}01$)β-Ga_2O_3, and calculate the band gap of the strained Al_2O_3 on ($\bar{2}01$) β-Ga_2O_3. The obtained value is 6.86 eV, which is in excellent agreement with the experimental value of 6.9 eV measured in Ref. [17].

To model the interface between α-Al_2O_3 and β-Ga_2O_3, we follow the epitaxial relationships of α-Al_2O_3 [100] ‖ β-Ga_2O_3 [102] and α-Al_2O_3 [120] ‖ β-Ga_2O_3 [010]. We construct an orthorhombic supercell comprising a α-Al_2O_3 slab with (3×1) in-plane periodicity and a β-Ga_2O_3 slab with (1×3) in-plane periodicity. In the interface models, the x and y are parallel to the [102] and [010] crystal axes of β-Ga_2O_3, respectively. The in-plane lattice mismatches are −2.2% and −9.4% along the x and y directions, respectively. The z axis is perpendicular to the ($\bar{2}01$) surface of β-Ga_2O_3 for all the interface models. When modeling the κ-Al_2O_3/β-Ga_2O_3 interface, we use the epitaxial relationships of κ-Al_2O_3 [100] ‖ β-Ga_2O_3 [102] and κ-Al_2O_3 [010] ‖ β-Ga_2O_3 [010]. The in-plane periodicities for the κ-Al_2O_3 slab and β-Ga_2O_3 slab are (3×1) and (1×3), respectively, which gives rises to the lattice mismatches of −1.9% and −8.2% along the in-plane x and y directions, respectively. In the case of the θ-Al_2O_3/β-Ga_2O_3 interface, we adopt the epitaxial relationships of θ-Al_2O_3 [102] ‖ β-Ga_2O_3 [102] and θ-Al_2O_3 [010] ‖ β-Ga_2O_3 [010]. The orthorhombic interface model contains a (1×3) slab and a (1×3) β-Ga_2O_3 slab. The corresponding in-plane lattice mismatches are −2.4% and −3.5% for the x and y directions, respectively. For the γ-Al_2O_3/β-Ga_2O_3

TABLE II. Lattice constants, band gaps, and VBM levels vs the bulk reference levels of the Al_2O_3 cells strained to the β-Ga_2O_3 substrate.

Strained Substrate	α-Al_2O_3 β-Ga_2O_3	κ-Al_2O_3 β-Ga_2O_3	θ-Al_2O_3 β-Ga_2O_3	γ-Al_2O_3 β-Ga_2O_3
a (Å)	4.91	4.91	14.72[a]	9.81
b (Å)	9.18	9.18	3.06	12.24
c (Å)	12.81	8.80	5.71	13.73
β			128.17°	
PBE0(α)	0.30	0.29	0.29	0.39
E_{gap}^{direct} (eV)	6.86	6.67	6.94	6.89
$E_{gap}^{indirect}$ (eV)			6.90	
VBM	3.57	3.35	2.97	2.56

[a]This is the lattice constants along the [102] direction.

interface, we consider the epitaxial relationships of γ-Al_2O_3 [120] ∥ β-Ga_2O_3 [102] and γ-Al_2O_3 [010] ∥ β-Ga_2O_3 [010]. To minimize the in-plane lattice mismatches, our orthorhombic slab is composed of a (3×1) γ-Al_2O_3 slab and a (2×2) β-Ga_2O_3 slab. This yields the lattice mismatches of 0.6% and −7.4% in the x and y directions, respectively. The determined epitaxial relationships between β-Ga_2O_3 and the four phases of Al_2O_3 are illustrated in Fig. S1 in the Supplemental Material [27]. For the considered four phases, the optimized lattice constants of the Al_2O_3 cells strained to the Ga_2O_3 substrate are listed in Table II. For α-Al_2O_3, the strained cell is orthorhombic in which the first two lattice constants (a and b) are same as the in-plane lattice distances in the corresponding interface model. In the case of θ-Al_2O_3, the lattice constant a in Table II denotes the in-plane distance along the [102] direction rather than along the [100] direction of the unit cell. We also provide the band gaps and the VBM positions through PBE0(α) calculations in which the mixing parameter α is same as that for strain-free Al_2O_3 bulk.

In the interface models, O atoms are used to connect the Al_2O_3 and the β-Ga_2O_3 slabs because O atoms can allow flexibility in bonding patterns [34]. For the surface Ga and Al atoms, there are no dangling bonds. After the epitaxial relationships between β-Ga_2O_3 and Al_2O_3 are determined, the third lattice vector of Ga_2O_3, the one out of the interface plane, is not parallel to any crystallographic directions of Al_2O_3, which hinders the use of superlattices to model the interfaces. Thick vacuum layers (∼20 Å) are added in the interface model (∼60 Å) to minimize the periodic image interactions in DFT calculations. Our interface models satisfy the electron-counting rule [48–51]. Take the α-Al_2O_3/β-Ga_2O_3 interface model as an example, each Ga or Al cation layer contains 12 Ga^{3+} or Al^{3+} ions, respectively, and each O anion layer contains 18 O^{2+} ions corresponding to −36 charges. The surface Ga and Al layers contribute +36 charges and therefore exactly neutralize the interfacial O layer. The O atoms in the top and bottom layers are passivated by the hydrogen atoms and have negligible effect on the interface lineup, which was obtained by extrapolating the macroscopically averaged electrostatic potential from the bulk-like regions to the nominal interface positions [34]. After performing full geometry optimizations in the interface models, we calculate the electronic structures at the GGA level. The interface models are shown in Fig. 2. The corresponding averaged electrostatic potential profiles are shown in Fig. 3. The planar average electrostatic potential represents the electrostatic potential averaged in the xy plane [i.e., the ($\bar{2}01$) surface of β-Ga_2O_3] and then a double convolution is applied along the z direction vertical to the xy plane to get rid of oscillations. We then use the alignment procedure to obtain the interface lineups. The calculated interface lineups are given in Table IV.

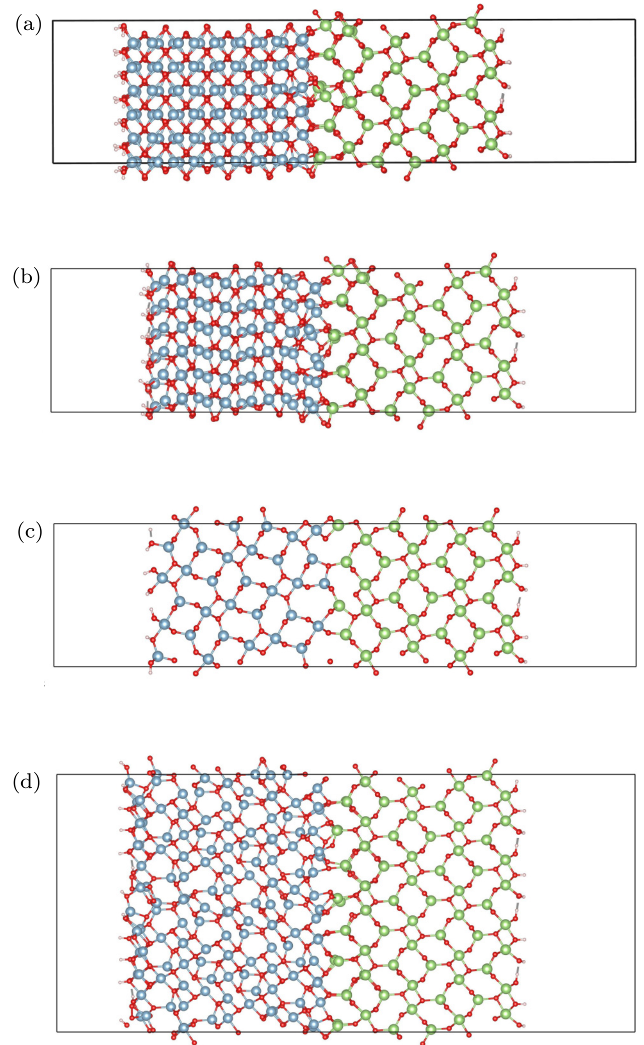

FIG. 2. Atomistic models of the Al_2O_3/β-Ga_2O_3 interfaces obtained from structural relaxations at the GGA level. (a) α-Al_2O_3/β-Ga_2O_3 interface, (b) κ-Al_2O_3/β-Ga_2O_3 interface, (c) θ-Al_2O_3/β-Ga_2O_3 interface, and (d) γ-Al_2O_3/β-Ga_2O_3 interface.

We also consider the situation in which Al_2O_3 is used as the substrate. The strain effects on the lattice constants, and the corresponding band gaps, and the VBM levels of β-Ga_2O_3 have to be accounted for. To achieve this, we convert the conventional unit cell of β-Ga_2O_3 into a larger monoclinic one with the ($\bar{2}01$) face [34]. The mathematical relationship between the first lattice vector $\mathbf{a'}$ of the larger cell and $\mathbf{a}$ of the conventional unit cell can be represented by the equation: $\mathbf{a'} = \mathbf{a} + 2\mathbf{c}$ [34]. The other two lattice vectors remain unchanged and the angle between $\mathbf{a'}$ and $\mathbf{c}$ is denoted as β' [34]. This transformed monoclinic unit cell [cf. Fig. 1(f)] is then strained

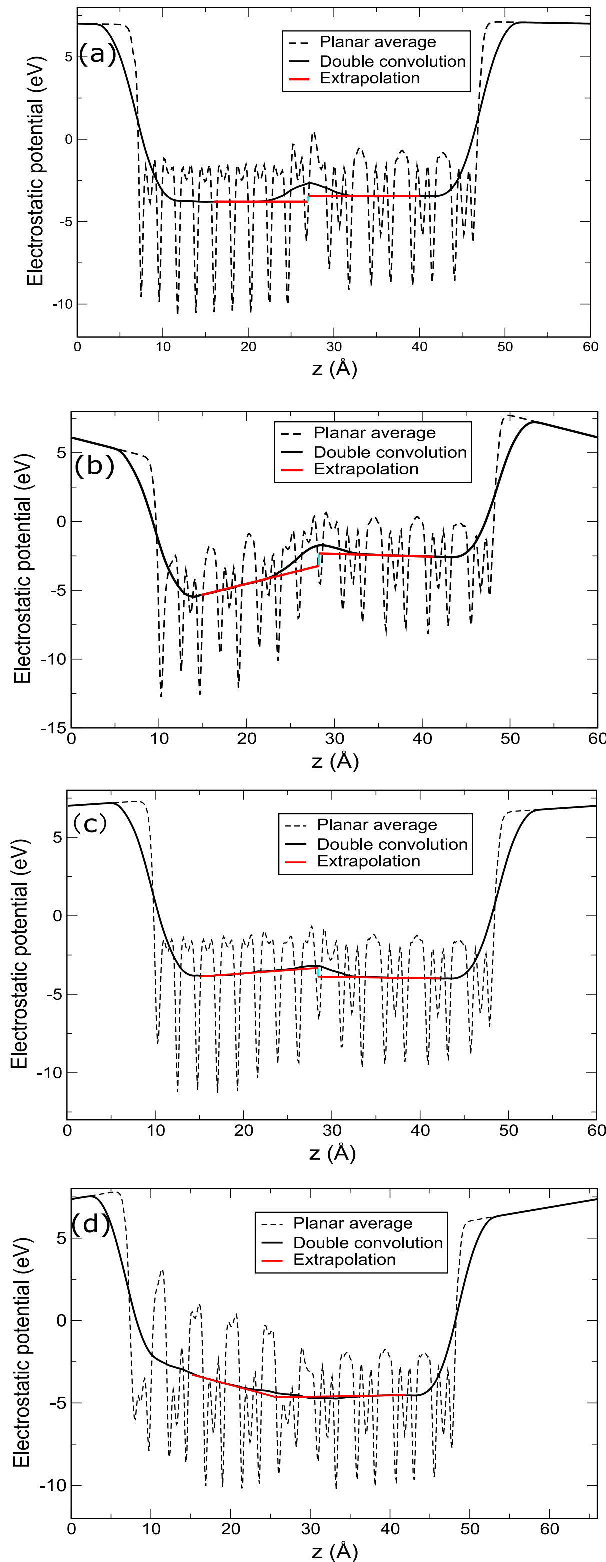

FIG. 3. Averaged electrostatic potential files for the (a) α-Al_2O_3/β-Ga_2O_3, (b) κ-Al_2O_3/β-Ga_2O_3, (c) θ-Al_2O_3/β-Ga_2O_3, and (d) γ-Al_2O_3/β-Ga_2O_3 interfaces calculated at the GGA level.

to the Al_2O_3 substrate, which determines the in-plane lattice constants (a' and b). The other lattice parameters (c and β') and the internal coordinates are optimized through structural relaxations [34]. The calculated lattice parameters, band gaps, and the VBM levels of β-Ga_2O_3 corresponding to different Al_2O_3 substrates are summarized in Table III. The Fock exchange parameter for the unstrained bulk, i.e., $\alpha = 0.27$, is adopted. The band gaps of the strained β-Ga_2O_3 cells at compressed volumes are larger than that of the unstrained bulk, which is consistent with the deformation potentials of β-Ga_2O_3 [60]. For the β-Ga_2O_3/Al_2O_3 interfaces, we perform structural relaxations and then determine the corresponding interface lineups as summarized in Table IV.

TABLE III. Lattice constants, band gaps, and VBM levels relative to the bulk reference levels of the strained β-Ga_2O_3 on the Al_2O_3 substrates.

Strained Substrate	β-Ga_2O_3 α-Al_2O_3	β-Ga_2O_3 κ-Al_2O_3	β-Ga_2O_3 θ-Al_2O_3	β-Ga_2O_3 γ-Al_2O_3
a' (Å)	14.41	14.64	14.37	14.80
b (Å)	2.79	2.81	2.95	2.83
c (Å)	5.83	5.81	5.83	5.80
β'	56.07°	55.73°	54.97°	55.33°
PBE0(α)	0.27	0.27	0.27	0.27
$E_{\mathrm{gap}}^{\mathrm{direct}}$ (eV)	5.35	5.32	5.15	5.28
VBM	3.88	3.63	3.42	3.46

The calculated band offsets together with the available experimental and theoretical results at the interfaces between β-Ga_2O_3 and Al_2O_3 are given in Table IV. Note the signs of the literature results are adjusted according to the definitions of VBO and CBO in Sec. II. The calculated valence and conduction band offsets are shown in Fig. 4. For α-Al_2O_3 on β-Ga_2O_3, the calculated VBO of 0.30 eV and CBO of 2.36 eV favor the middle of the range of the experimentally measured offsets [16–18]. The differences between the theoretically and experimental values could be attributed to epitaxial relationships, strain, and interfacial defects, etc. [1]. In Ref. [16], (010) β-Ga_2O_3 rather than ($\bar{2}01$) β-Ga_2O_3 is taken as the substrate, which could lead to different epitaxial

TABLE IV. Calculated interface lineup (in eV) and band offsets (in eV) at the interfaces between β-Ga_2O_3 and Al_2O_3. The available experimental and theoretical results are also given.

Interface	Interface lineup	VBO	CBO
α-Al_2O_3/β-Ga_2O_3	–0.33	0.30	2.36
Expt. [16]		–0.70	1.50
Expt. [17]		–0.07	2.23
Expt. [17]		0.86	3.16
Expt. [18]			1.7
Calc. [9]		–0.27	3.68
κ-Al_2O_3/β-Ga_2O_3	–0.91	–0.40	1.46
θ-Al_2O_3/β-Ga_2O_3	0.55	0.54	2.63
Calc. [9]		0.37	2.74
γ-Al_2O_3/β-Ga_2O_3	0.04	–0.34	1.74
Expt. [19]		–0.5	1.9
β-Ga_2O_3/α-Al_2O_3	1.17	0.97	–2.46
β-Ga_2O_3/κ-Al_2O_3	0.19	–0.04	–2.39
β-Ga_2O_3/θ-Al_2O_3	–0.24	0.14	–2.32
β-Ga_2O_3/γ-Al_2O_3	–0.23	0.03	–2.29

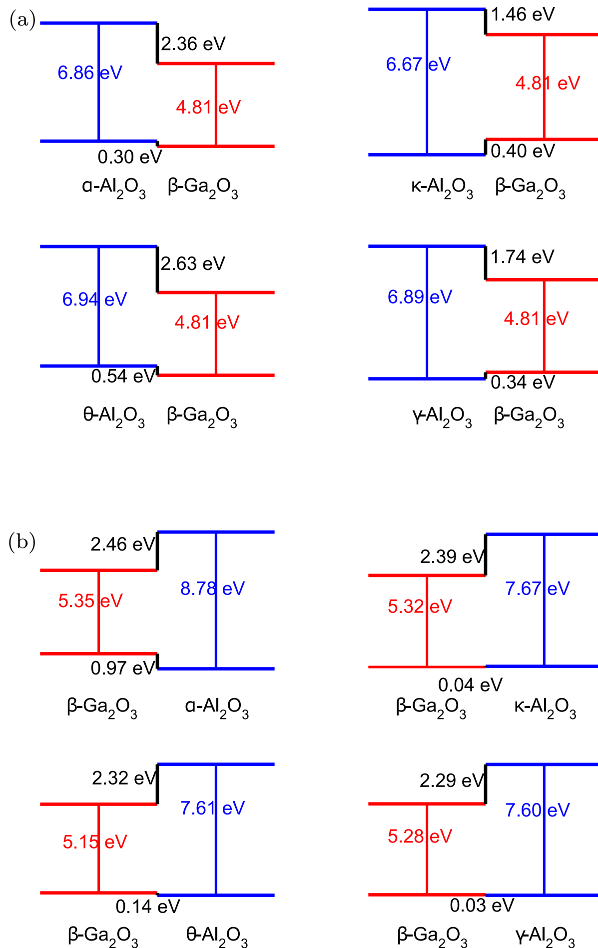

FIG. 4. Band alignment diagrams of the interfaces between β-Ga_2O_3 and Al_2O_3. In (a) and (b), the substrates are Ga_2O_3 and Al_2O_3, respectively. The signs of the offsets are dropped out for brevity. (a) Al_2O_3/β-Ga_2O_3 interface and (b) β-Ga_2O_3/Al_2O_3 interface.

relationships and strain conditions. In Ref. [18], the CBO is extracted from capacitance-voltage measurements at the interface. We suggest that α-Al_2O_3 films are thick enough ($\geqslant$12 nm) to give rise to dislocations and thus deviate from the value at the interface. We note the calculate band offsets are closer to those measured for ALD than sputtered α-Al_2O_3 on β-Ga_2O_3 in Ref. [17]. This is consistent with the fact that sputtering could cause more interfacial disorder and defects than ALD [17]. Recently, Peelaers *et al.* calculated a VBO of -0.27 eV and a CBO of 3.68 eV between unstrained α-Al_2O_3 and β-Ga_2O_3 bulks from the electron affinity rule [9]. The differences from our results partly because that we explicitly consider the strain effects. For κ-Al_2O_3/β-Ga_2O_3, we obtain a VBO of -0.40 eV and a CBO of 1.46 eV. In the case of the θ-Al_2O_3/interface, the calculated VBO and CBO are 0.54 eV and 2.63 eV, respectively. For this interface, Peelaers *et al.* calculated a VBO of 0.37 eV and a CBO of 2.74 eV between unstrained θ-Al_2O_3 and β-Ga_2O_3 by assuming the electron affinity rule [9]. This good agreement is attributed to the fact that the lattice mismatches between θ-Al_2O_3 and β-Ga_2O_3 are rather small and the interface model satisfies the electron counting rule. For γ-Al_2O_3 on β-Ga_2O_3, the calculated VBO of -0.34 eV is in good agreement with the experimental value of -0.5 eV for γ-Al_2O_3 on (010) β-Ga_2O_3 reported by Hattori *et al.* [19]. This good agreement is partly due to the satisfaction of the electron counting rule in our models despite the fact that the surfaces involved of β-Ga_2O_3 are different. For Al_2O_3 on β-Ga_2O_3, the α and θ phases form type II heterojunctions. For κ-Al_2O_3 and γ-Al_2O_3 on $(\bar{2}01)\beta$-Ga_2O_3, there are type I band alignments but the corresponding VBOs are less than 1 eV, thereby indicating not very sufficient barriers for holes.

We then discuss the band alignments of β-Ga_2O_3 on Al_2O_3. For β-Ga_2O_3/α-Al_2O_3, we obtain a VBO of 0.97 eV and a CBO of -2.46 eV. Both the CBO and the VBO are $\gtrsim$1 eV, therefore we identify α-Al_2O_3 as an appropriate candidate for gate dielectrics on β-Ga_2O_3 in MOSFETs. For β-Ga_2O_3 on κ-, θ-, and γ-Al_2O_3, we find that the VBOs are nearly negligible but the CBOs are $\sim$2.4 eV indicating sufficient barriers for electrons. Hence, these three phase of Al_2O_3 can be used as electron blocking layers in β-Ga_2O_3-based LEDs [61].

IV. CONCLUSIONS

In summary, we studied the band offsets at the interfaces between $(\bar{2}01)$ β-Ga_2O_3 and the four representative phases of Al_2O_3 (α, κ, θ, and γ) through the state-of-the-art hybrid density functional calculations. The calculated band offsets are in line with the available experimental results. The modeling procedures in this study can directly be applied to the interfaces between β-Ga_2O_3 and technologically promising $(Al_xGa_{1-x})_2O_3$ alloys [9,47], and be useful for the study of the interfaces involving (010) β-Ga_2O_3. More generally, the present study shows how to address band alignments at the interfaces between β-Ga_2O_3 with oxides. The calculated band alignments are essential for the device designs based on β-Ga_2O_3 such as MOSFETs and LEDs.

ACKNOWLEDGMENTS

The author would like to thank Prof. Walter R. L. Lambrecht for the fruitful discussions. This work was financially supported by Natural Science Foundation of Shandong Province (Grant No. ZR2022QA077) and Taishan Scholar Program of Shandong Province. This work was supported by National Supercomputer Center in Guangzhou.

[1] S. J. Pearton, J. Yang, P. H. Cary, F. Ren, J. Kim, M. J. Tadjer, and M. A. Mastro, Appl. Phys. Rev. **5**, 011301 (2018).
[2] M. Higashiwaki, K. Sasaki, A. Kuramata, T. Masui, and S. Yamakoshi, Appl. Phys. Lett. **100**, 013504 (2012).
[3] M. A. Mastro, A. Kuramata, J. Calkins, J. Kim, F. Ren, and S. J. Pearton, ECS J. Solid State Sci. Technol. **6**, P356 (2017).
[4] A. Kuramata, K. Koshi, S. Watanabe, Y. Yamaoka, T. Masui, and S. Yamakoshi, Jpn. J. Appl. Phys. **55**, 1202A2 (2016).

[5] W. H. Gitzen (ed.), *Alumina as a Ceramic Material* (American Ceramic Society, Westerville, OH, 2006).
[6] E. Dorre and H. Hubner, *Alumina*, Materials Research and Engineering (Springer, Berlin, 2011).
[7] I. Levin and D. Brandon, J. Am. Ceram. Soc. **81**, 1995 (2005).
[8] C.-K. Lee, E. Cho, H.-S. Lee, K. S. Seol, and S. Han, Phys. Rev. B **76**, 245110 (2007).
[9] H. Peelaers, J. B. Varley, J. S. Speck, and C. G. Van de Walle, Appl. Phys. Lett. **112**, 242101 (2018).
[10] T. Wang, W. Li, C. Ni, and A. Janotti, Phys. Rev. Appl. **10**, 011003(R) (2018).
[11] S. Mu and C. G. Van de Walle, Phys. Rev. Mater. **6**, 104601 (2022).
[12] K. D. Chabak, N. Moser, A. J. Green, D. E. Walker, Jr, S. E. Tetlak, E. Heller, A. Crespo, R. Fitch, J. P. McCandless, K. Leedy *et al.*, Appl. Phys. Lett. **109**, 213501 (2016).
[13] M. Higashiwaki, K. Sasaki, T. Kamimura, M. Hoi Wong, D. Krishnamurthy, A. Kuramata, T. Masui, and S. Yamakoshi, Appl. Phys. Lett. **103**, 123511 (2013).
[14] W. S. Hwang, A. Verma, H. Peelaers, V. Protasenko, S. Rouvimov, H. (Grace) Xing, A. Seabaugh, W. Haensch, C. Van de Walle, Z. Galazka *et al.*, Appl. Phys. Lett. **104**, 203111 (2014).
[15] S. Ahn, F. Ren, J. Kim, S. Oh, J. Kim, M. A. Mastro, and S. J. Pearton, Appl. Phys. Lett. **109**, 062102 (2016).
[16] T. Kamimura, K. Sasaki, M. H. Wong, D. Krishnamurthy, A. Kuramata, T. Masui, S. Yamakoshi, and M. Higashiwaki, Appl. Phys. Lett. **104**, 192104 (2014).
[17] P. H. Carey, F. Ren, D. C. Hays, B. Gila, S. Pearton, S. Jang, and A. Kuramata, Vacuum **142**, 52 (2017).
[18] T.-H. Hung, K. Sasaki, A. Kuramata, D. N. Nath, P. Sung Park, C. Polchinski, and S. Rajan, Appl. Phys. Lett. **104**, 162106 (2014).
[19] M. Hattori, T. Oshima, R. Wakabayashi, K. Yoshimatsu, K. Sasaki, T. Masui, A. Kuramata, S. Yamakoshi, K. Horiba, H. Kumigashira, and A. Ohtomo, Jpn. J. Appl. Phys. **55**, 1202B6 (2016).
[20] R. Shaltaf, G.-M. Rignanese, X. Gonze, F. Giustino, and A. Pasquarello, Phys. Rev. Lett. **100**, 186401 (2008).
[21] A. Alkauskas, P. Broqvist, F. Devynck, and A. Pasquarello, Phys. Rev. Lett. **101**, 106802 (2008).
[22] J. VandeVondele, M. Krack, F. Mohamed, M. Parrinello, T. Chassaing, and J. Hutter, Comput. Phys. Commun. **167**, 103 (2005).
[23] W. Kohn and L. J. Sham, Phys. Rev. **140**, A1133 (1965).
[24] J. VandeVondele and J. Hutter, J. Chem. Phys. **127**, 114105 (2007).
[25] S. Goedecker, M. Teter, and J. Hutter, Phys. Rev. B **54**, 1703 (1996).
[26] H. J. Monkhorst and J. D. Pack, Phys. Rev. B **13**, 5188 (1976).
[27] See Supplemental Material at http://link.aps.org/supplemental/10.1103/PhysRevMaterials.7.014603 for the epitaxial relationships between β-Ga_2O_3 and Al_2O_3 and more computational details.
[28] J. P. Perdew, K. Burke, and M. Ernzerhof, Phys. Rev. Lett. **77**, 3865 (1996).
[29] J. P. Perdew, M. Ernzerhof, and K. Burke, J. Chem. Phys. **105**, 9982 (1996).
[30] C. Adamo and V. Barone, J. Chem. Phys. **110**, 6158 (1999).
[31] M. Guidon, J. Hutter, and J. VandeVondele, J. Chem. Theory Comput. **6**, 2348 (2010).
[32] C. G. Van de Walle and R. M. Martin, Phys. Rev. B **34**, 5621 (1986).
[33] A. Baldereschi, S. Baroni, and R. Resta, Phys. Rev. Lett. **61**, 734 (1988).
[34] S. Lyu and A. Pasquarello, Appl. Phys. Lett. **117**, 102103 (2020).
[35] L. Weston, H. Tailor, K. Krishnaswamy, L. Bjaalie, and C. G. Van de Walle, Comput. Mater. Sci. **151**, 174 (2018).
[36] K. Steiner, W. Chen, and A. Pasquarello, Phys. Rev. B **89**, 205309 (2014).
[37] S. Baroni, R. Resta, A. Baldereschi, and M. Peressi, in *NATO ASI Series* (Springer, New York, 1989), pp. 251–271.
[38] L. Bengtsson, Phys. Rev. B **59**, 12301 (1999).
[39] D. H. Foster and G. Schneider, arXiv:1403.5230.
[40] B. Ollivier, R. Retoux, P. Lacorre, D. Massiot, and G. Férey, J. Mater. Chem. **7**, 1049 (1997).
[41] Y. Yourdshahyan, C. Ruberto, M. Halvarsson, L. Bengtsson, V. Langer, B. I. Lundqvist, S. Ruppi, and U. Rolander, J. Am. Ceram. Soc. **82**, 1365 (2004).
[42] R.-S. Zhou and R. L. Snyder, Acta Cryst. B **47**, 617 (1991).
[43] Ľ. Smrčok, V. Langer, and J. Křesťan, Acta Cryst. C **62**, i83 (2006).
[44] M. Yazdanmehr, S. J. Asadabadi, A. Nourmohammadi, M. Ghasemzadeh, and M. Rezvanian, Nanoscale Res. Lett. **7**, 488 (2012).
[45] C. Wolverton and K. C. Hass, Phys. Rev. B **63**, 024102 (2000).
[46] S. Geller, J. Chem. Phys. **33**, 676 (1960).
[47] A. Ratnaparkhe and W. R. L. Lambrecht, Phys. Status Solidi (b) **257**, 1900317 (2020).
[48] P. W. Peacock and J. Robertson, Phys. Rev. Lett. **92**, 057601 (2004).
[49] J. Robertson and L. Lin, Appl. Phys. Lett. **99**, 222906 (2011).
[50] L. Lin and J. Robertson, Appl. Phys. Lett. **98**, 082903 (2011).
[51] Z. Zhang, Y. Guo, and J. Robertson, Appl. Phys. Lett. **114**, 161601 (2019).
[52] P. Broqvist, J. F. Binder, and A. Pasquarello, Appl. Phys. Lett. **94**, 141911 (2009).
[53] D. Colleoni, G. Miceli, and A. Pasquarello, Appl. Phys. Lett. **107**, 211601 (2015).
[54] M. Lucht, M. Lerche, H.-C. Wille, Y. V. Shvyd'ko, H. D. Rüter, E. Gerdau, and P. Becker, J. Appl. Cryst. **36**, 1075 (2003).
[55] M. Halvarsson, V. Langer, and S. Vuorinen, Surf. Coat. Technol. **76-77**, 358 (1995).
[56] J. Åhman, G. Svensson, and J. Albertsson, Acta Cryst. C **52**, 1336 (1996).
[57] R. H. French, J. Am. Ceram. Soc. **73**, 477 (1990).
[58] E. O. Filatova and A. S. Konashuk, J. Phys. Chem. C **119**, 20755 (2015).
[59] T. Matsumoto, M. Aoki, A. Kinoshita, and T. Aono, Jpn. J. Appl. Phys. **13**, 1578 (1974).
[60] J. E. N. Swallow, R. G. Palgrave, P. A. E. Murgatroyd, A. Regoutz, M. Lorenz, A. Hassa, M. Grundmann, H. von Wenckstern, J. B. Varley, and T. D. Veal, ACS Appl. Mater. Interfaces **13**, 2807 (2021).
[61] C.-H. Lin and C.-T. Lee, J. Lumin. **224**, 117326 (2020).